AIP | Journal of Applied Physics

Open volume defects and magnetic phase transition in Fe60Al40 transition metal aluminide

M. O. Liedke, W. Anwand, R. Bali, S. Cornelius, M. Butterling, T. T. Trinh, A. Wagner, S. Salamon, D. Walecki, A. Smekhova, H. Wende, and K. Potzger

Citation: Journal of Applied Physics **117**, 163908 (2015); doi: 10.1063/1.4919014
View online: http://dx.doi.org/10.1063/1.4919014
View Table of Contents: http://scitation.aip.org/content/aip/journal/jap/117/16?ver=pdfcov
Published by the AIP Publishing

JOURNAL OF APPLIED PHYSICS **117**, 163908 (2015)

Open volume defects and magnetic phase transition in $Fe_{60}Al_{40}$ transition metal aluminide

M. O. Liedke,[1,a)] W. Anwand,[1] R. Bali,[2] S. Cornelius,[2] M. Butterling,[1] T. T. Trinh,[1,3] A. Wagner,[1] S. Salamon,[4] D. Walecki,[4] A. Smekhova,[4] H. Wende,[4] and K. Potzger[2]
[1]*Institute of Radiation Physics, Helmholtz-Zentrum Dresden - Rossendorf, Bautzner Landstraße 400, 01328 Dresden, Germany*
[2]*Institute of Ion Beam Physics and Materials Research, Helmholtz-Zentrum Dresden - Rossendorf, Bautzner Landstraße 400, 01328 Dresden, Germany*
[3]*Technical University Dresden, Helmholtzstr. 10, 01609 Dresden, Germany*
[4]*Faculty of Physics and Center for Nanointegration Duisburg-Essen (CENIDE), University of Duisburg-Essen, Lotharstraße 1, 47048 Duisburg, Germany*

(Received 19 February 2015; accepted 13 April 2015; published online 24 April 2015)

Magnetic phase transition in the $Fe_{60}Al_{40}$ transition metal aluminide from the ferromagnetic disordered A2-phase to the paramagnetic ordered B2-phase as a function of annealing up to 1000 °C has been investigated by means of magneto-optical and spectroscopy techniques, i.e., Kerr effect, positron annihilation, and Mössbauer spectroscopy. The positron annihilation spectroscopy has been performed *in-situ* sequentially after each annealing step at the Apparatus for *In-situ* Defect Analysis that is a unique tool combining positron annihilation spectroscopy with temperature treatment, material evaporation, ion irradiation, and sheet resistance measurement techniques. The overall goal was to investigate the importance of the open volume defects onto the magnetic phase transition. No evidence of variation in the vacancy concentration in matching the magnetic phase transition temperature range (400–600 °C) has been found, whereas higher temperatures showed an increase in the vacancy concentration. © *2015 AIP Publishing LLC*.
[http://dx.doi.org/10.1063/1.4919014]

I. INTRODUCTION

Transition metal (TM) intermetallics, especially TM aluminides like $Fe_{60}Al_{40}$, combine remarkable functional structural and peculiar magnetic properties, e.g., good corrosion resistance in an aggressive environment, structural stability at elevated temperatures, and the ordering dependent magnetic phase transition, respectively.[1,2] Magnetic ordering plays here an important role, where for ordered iron aluminides the magnetic moment decreases with increasing Al content until the alloy turns paramagnetic at about 30 at. % of Al. Second, disordered iron aluminides feature a large magnetic moment at room temperature despite Al content higher than about 35 at. %.[3,4] Moreover, in the case of chemically ordered paramagnetic (B2-phase) iron aluminides with Al content larger than about 30 at. % atomic intermixing induces room temperature disorder driven ferromagnetism (A2-phase).[5] That intermixing induced phase transition can be realized in many ways, i.e., by ion irradiation,[6,7] ball milling,[2] mechanical alloying,[8] deformation techniques like a high pressure compression[9] or cold working procedures.[10] Qualitatively, the phase transition from the chemically ordered B2-phase to disordered ferromagnetic A2-phase is explained theoretically by the so-called *local environment model,*[11] which presumes the magnetic moment of an atom as a superposition of magnetic moments of the same kind nearest neighbor atoms. Thus, the magnetic moment of the A2 disorder phase is larger due to the higher number of Fe-Fe nearest neighbors (on average 4.8) compared to the B2 ordered phase (on average 2.67).[12] Although, the nearest neighbors interactions describes the magnetic phase transition reasonably well, different contributing mechanisms has been suggested, too. For example, variations of the lattice parameter[8,13] or defects may play a role.[14–16] The A2 FeAl phase consists mostly of high concentration single vacancies, whereas the B2 ordered phase is dominated by more complex type of defects, i.e., triple defects at low temperatures and double vacancies at higher temperatures.[14,15] High concentration of complex vacancies in the ordered FeAl can possibly accelerate the phase transition process to the A2-phase if the material is exposed to, for example, ion irradiation due to (i) increased thermal diffusion of the host atoms throughout vacancies, and (ii) dissociation of complex vacancies into single vacancies. The scope of this manuscript is to assess the influence of the open volume defects on the $Fe_{60}Al_{40}$ transition metal aluminides magnetic phase transition from the ferromagnetic A2-phase to the paramagnetic B2-phase by thermal annealing up to 1000 °C ($T_{melt} = 1234$ °C).

The following techniques have been utilized for assessing the magnetic properties: (i) longitudinal Magneto-Optical Kerr Effect (MOKE) and (ii) Conversion Electron Mössbauer Spectroscopy (CEMS). X-ray diffraction (XRD) patterns were collected using a PANalytical Empyrean diffractometer with Cu-Ka radiation in 1° grazing incidence angle geometry. A Xe proportional detector equipped with a parallel plate collimator was used to collect diffracted X-rays from an illuminated sample area of $8 \times 10\,mm^2$. The

a)Author to whom correspondence should be addressed. Electronic mail: m.liedke@hzdr.de

sample topography after 1000 °C annealing was imaged by means of Scanning Electron Microscopy (SEM).

The manuscript consists of Secs. I–IV: (I) introduction, (II) sample preparation and experimental procedure, (III) results and discussion, and (IV) conclusion.

II. SAMPLE PREPARATION AND EXPERIMENTAL PROCEDURE

Two identical $Fe_{60}Al_{40}$ thin films have been sputter-deposited (deposition rate of about 0.03 nm/s) at room temperature (RT) on a $1 \times 1\,cm^2$ silicon substrate. Silicon substrates with a native oxide layer of about 100 nm thickness have been utilized in order to prevent intermixing with the metallic film during annealing. The alloy thickness of about 250 nm has been chosen to account for the optimal depth profile distribution of implanted positrons [see Fig. 3(a)]. The as-grown films are chemically disordered, i.e., of the A2-phase, and vacuum annealing at 773 K transformed the films into the ordered B2-phase. The disordered ferromagnetic sample has been annealed in the 30–1000 °C temperature range, thus close to the $Fe_{60}Al_{40}$ melting point, and sequentially measured *in-situ* by means of Variable Energy Positron Annihilation Spectroscopy (VEPAS) at the Apparatus for In-situ Defect Analysis (AIDA).

AIDA is a unique high vacuum system (base pressure of 7×10^{-9} mbar) that combines several experimental techniques, i.e., ion irradiation, metal evaporation, temperature treatment, sheet resistance and PAS measurements, targeting on defect tailoring and defect analysis. AIDA has been manufactured by the PREVAC® (PREVAC sp. z o.o., Raciborska Str. 61, 44-362 Rogów, Poland (http://www.prevac.eu/)) company, and it is located at an end-station of Slow-Positron System of Rossendorf (SPONSOR) that provides a tungsten moderated and magnetically guided variable energy positron beam extracted from a ^{22}Na source.[17,18] The energy of incident positrons is in general varied in the range of 0.03–36 keV. The coincident Doppler broadening (cDB) of the annihilation line at fixed energy is performed by two High-Purity Germanium (HPGe) detectors with energy resolution of (780 ± 20) eV at 511 keV, whereas the standard single HPGe detector Doppler broadening (sDB) with an energy resolution of (1.09 ± 0.01) keV is usually utilized for the energy scans.

AIDA provides similar energy resolution as SPONSOR, however, the annihilation count rate is lower by 20%–30% due to the more massive manipulator sample holder. In general, AIDA offers various defect analysis and modification methods. First, metallic alloy thin films can be evaporated from up to four e-beam evaporators and/or effusion cells. During or after evaporation, the films can be exposed to ion beam irradiation at energies up to 5 keV in order to induce defects. Noble gases and also reactive gases can be employed. Defects can be thermally annealed (up to about 1300 K) or stabilized (down to about 50 K). Finally, defects can be analyzed by PAS and the sheet resistance 4-point Van der Pauw method at the same time. Ion irradiation, metal evaporation, temperature treatment, and defect analysis can be performed sequentially or simultaneously. For this particular experiment, we have utilized only a fraction of AIDA capabilities namely, the temperature treatment and PAS.

First, the as-grown ordered and disordered $Fe_{60}Al_{40}$ samples were measured by means of MOKE, XRD, CEMS, Variable Energy sDB (VEsDB), and cDB for reference. Next, the disordered $Fe_{60}Al_{40}$ has been sequentially annealed in vacuum for about 5 h each temperature step at AIDA in the temperature range of 400–1000 °C (annealing ramp about 20 °C/min). After each annealing step the sample was cooled (cooling ramp about 30 °C/min) to room temperature (RT) and transferred *ex-situ* for MOKE, VEsDB, and cDB measurements. The cDB of the annihilation line was performed at SPONSOR at fixed energy of 5 keV because of the higher count rate, whereas the VEsDB scans have been done back at AIDA. In addition, the sample was investigated by XRD after 600 °C and 1000 °C, and by CEMS and SEM at 1000 °C only.

III. RESULTS AND DISCUSSION

A. MOKE and SEM

Magneto-optical measurements of the ordered $Fe_{60}Al_{40}$ as well as disordered sample after each annealing step have been done *ex-situ* at room temperature. A set of magnetization reversal loops is presented in Figure 1. The ordered sample shows no magnetic signal at room temperature at all, whereas the disordered one is represented by a magnetic reversal curve with coercivity of about 65 Oe. The shape of the curve suggests a distribution of the magnetic domain sizes possibly related to the grain size distribution. Due to annealing both the remanence and coercivity drop significantly and already at 500 °C the magnetic signal vanishes. Following the annealing steps the magnetic reversal curves show: (i) sharper reversal transitions, thus more mono-domain like behavior (300 °C), (ii) a paramagnetic loop with low remanence and magnetization saturation (400 °C), and (iii) a straight line in the 500–1000 °C temperature range. At 500 °C and at the maximum temperature the $Fe_{60}Al_{40}$ film, which melted was evidenced by Scanning Electron

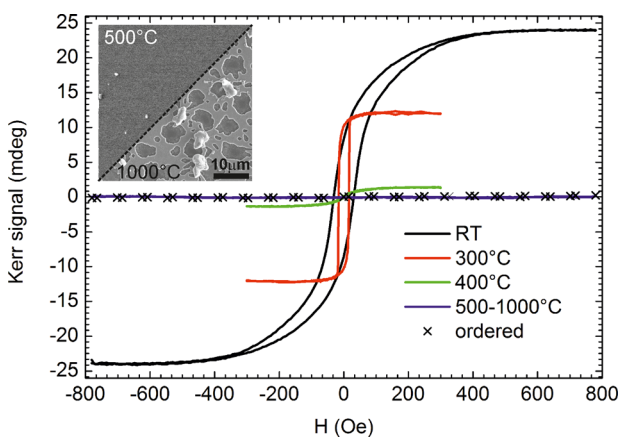

FIG. 1. Magneto-optical Kerr effect magnetization reversal loops of the disordered $Fe_{60}Al_{40}$ alloy measured *ex-situ* at RT after subsequent annealing and cooling down to room temperature. SEM images from the 500 °C and 1000 °C annealed samples (inset). Dewetting of the FeAl layer with possible Al segregation into steep islands is visible.

Microscopy (SEM) (see inset of Fig. 1). The SEM images reveal continuous film surface at 500 °C, whereas at 1000 °C darker and bright island-like regions were found that possibly correspond to the former FeAl film and Al-AlO segregations, respectively. The light gray color surrounding the island-like regions in the 1000 °C case represents most probably the SiO_2 substrate.

B. XRD

Figure 2 shows the XRD patterns of the as-grown (partially disordered, ferromagnetic), the 600 °C annealed (fully ordered, paramagnetic) and the 1000 °C annealed FeAl sample, respectively. The effect of vacuum annealing at 600 °C is visible in terms of (i) intense super lattice peaks (SLPs) indicating a high degree of chemical ordering in the $Fe_{60}Al_{40}$ (B2 structure, PDF #33–0020), (ii) narrowing of the related diffraction peaks, indicating crystallite growth and/or decrease of micro-strain, and (iii) shift of all peaks to higher 2θ angles indicating a decrease of lattice constant upon annealing. After annealing at 1000 °C further decrease of the lattice constant has been observed. The role of the lattice cell reduction in the recovery of the paramagnetic behavior is still under debate. For example, band structure calculations and XMCD measurements under pressure for ball milled disordered $Fe_{60}Al_{40}$ systems show concomitant magnetic moment and lattice parameter reduction.[2] In some studies mainly focused onto the B2 → A2 magnetic phase transition during high pressure compression a correlation between structural and magnetic properties has been shown indicating that the induced ferromagnetism is controlled by both the lattice cell expansion and nearest-neighbor interactions.[9] At the same time, a second set of diffraction peaks at angular positions close to that of Fe (bcc structure, PDF #060696) is visible indicating the formation of another phase with bcc symmetry upon 1000 °C annealing. The nature of this phase remains to be identified, but the peak positions do not correspond to neither $FeAl_3$ (fcc structure, PDF#50-0955) nor any of the other equilibrium phases in the Fe-Al phase diagram.[19] Moreover, detailed analysis of the 1000 °C annealed film shows evidence for Fe silicide formation at the Fe-SiO_2 interface with weak diffraction peaks corresponding to FeSi (cubic, PDF#38-1397) and $FeSi_2$ (tetragonal, PDF#35-0822). In addition, a phase separation into bcc alpha-Fe with some dissolved Al ~10%–20% and FeAl-B2 at 1000 °C is possible as well as a tetragonal distortion of FeAl-B2 at both 600 °C and 1000 °C (no uniform peak shift) due to thermal expansion coefficient mismatch between film and substrate.

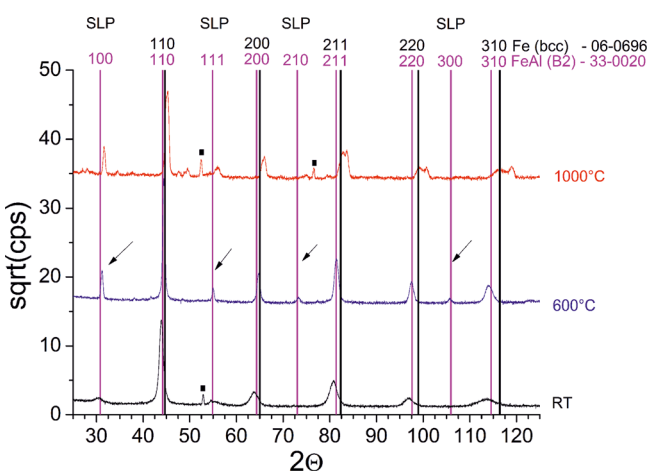

FIG. 2. Grazing incidence angle XRD patterns of the disordered $Fe_{60}Al_{40}$ sample measured prior the annealing at RT, after 600 °C, and 1000 °C annealing.

C. PAS

Two different positron annihilation spectroscopy (PAS) measurement types have been utilized for defect analysis after each temperature step: (i) room temperature standard Doppler broadening as a function of positron energy E for depth profiling [Fig. 4(a)], (ii) RT coincident Doppler broadening measurements at fixed energy after each temperature step that can in detail reveal information of the chemical environment of defects with higher energy resolution [Fig. 4(b)]. In both cases two specific annihilation line parameters have been extracted: (i) the shape parameter S that corresponds to the fraction of positrons annihilating with the low-momentum electrons localized close to the middle of the annihilation line, and (ii) the wing parameter W that takes into appoint positron annihilation with high-momentum electrons at the outer region of the annihilation line. In general, the S parameter is sensitive to the open volume defects amount and their size, whereas the W parameter is a fingerprint of the annihilation site chemical environment, thus defects decoration by neighboring matrix elements. For more details refer to Ref. 20.

First, in order to estimate the optimum positron energy conditions for the $Fe_{60}Al_{40}$ annealing procedure, the Makhov positron implantation depth profiles have been simulated [Fig. 3(a)]. For monoenergetic positrons of energy E and the implantation depth d, the depth profile can be calculated as follows:[21]

$$P(d,E) = \frac{m d^{m-1}}{d_0^m} \exp\left[-\left(\frac{d}{d_0}\right)^m\right], \; d_0 = \frac{AE^r}{\rho\Gamma\left(1+\frac{1}{m}\right)}, \quad (1)$$

where $m = 2$, $r = 1.62$, and $A = 36\,\mu\mathrm{g cm^{-2} keV^{-r}}$ are empirical values, $\rho = 5.9\ \mathrm{g \times cm^{-3}}$ is the FeAl density, and Γ is a gamma function. The positron distribution across the film thickness clearly broadens as a function of energy. In the low energy regime, up to about 3 keV the positron annihilation takes place mostly close to the surface and the positron distribution is sharp, whereas for larger energies of about 5 keV the whole layer thickness is covered, the maximum of the positron distribution coincides with about the middle of the magnetic layer, and the positron fraction in the substrate is negligible [Fig. 3(a)]. For energies larger than 5 keV, the positron fraction in the substrate increases and already at 8 keV the positron fraction in the substrate is about equal as in the film. Thus, positron energy $E = 5$ keV has been chosen for cDB measurements of disordered $Fe_{60}Al_{40}$ after annealing steps.

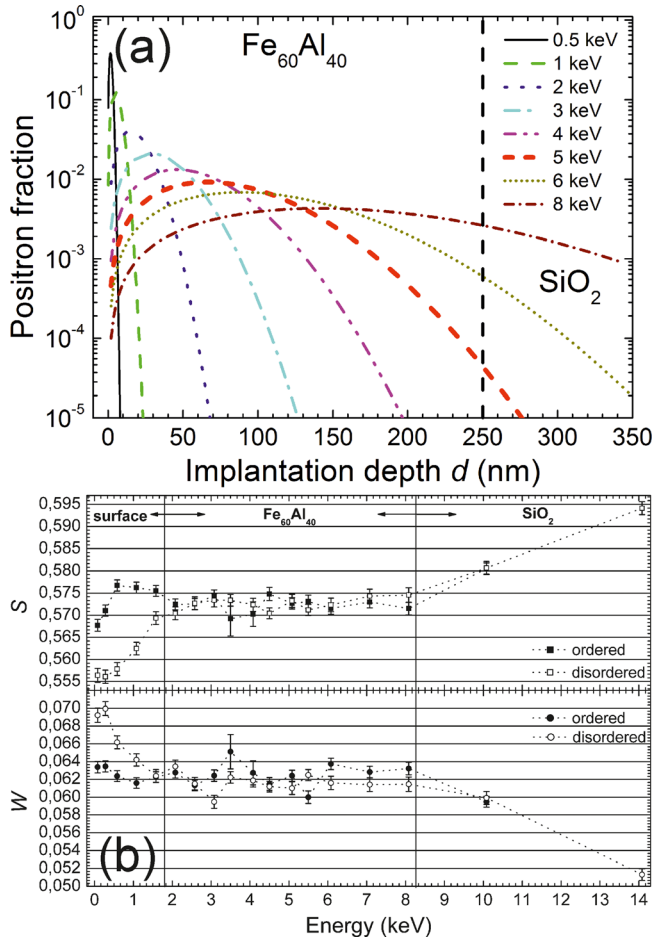

FIG. 3. Simulated Makhov positron implantation profiles for the FeAl alloy in the 0.5–8 keV energy range (a). The positron depth distribution covers the overall film thickness for E = 5 keV whereas only a very small positron fraction enters the SiO_2 substrate. Positron annihilation standard Doppler broadening parameters *S* (squares) and *W* (dots) as a function of positron energy prior annealing (b). The surface, magnetic layer, and substrate contributions can be recognized.

Prior to annealing both ordered and disordered samples were measured by means of sDB in the energy range of 0.08–14 keV. The annihilation line parameters *S* and *W* were extracted from the annihilation spectra for each energy step. The results are plotted in Figure 3(b). At the first glance no visible changes in the open volume and defect decoration were found since both *S* and *W* parameters are mostly constant within the FeAl film. In the low energy region up to about 2 keV that corresponds to the sample surface larger variation of *S* and *W* are visible. The disordered sample shows a longer tail in *S* and *W* before reaching the plateau bulk value. That is likely due to the variation in the oxide layer thickness, possibly lower roughness, and recrystallization in the annealed ordered sample compare to the as-deposited disordered one.[22] The middle of the plateau is located at about 5 keV that is in good agreement with the Makhov profiling [Fig. 3(a)]. In the high energy range, from about 8 keV a rather steep increase of *S* suggests larger positron annihilation contribution from the SiO_2 substrate. According to the Makhov profiling a transition between the film and the substrate should be visible already at about 6–7 keV. The fact that the larger positron annihilation contribution from the substrate is found at about 8 keV indicates: (i) about 20% larger the overall film thickness and/or (ii) a back diffusion of positrons from the substrate to the film, which is not taken into account by the Makhov model. Nevertheless, if the film thickness is indeed larger both the ordered and disordered samples show the same film-substrate transition behavior anyway.

As the next step, the disordered sample has been sequentially annealed in the 400–1000 °C temperature range and for each temperature step the sDB energy dependencies [Fig. 4(a)] as well as the cDB spectra at the positron energy of 5 keV [Fig. 4(b)] were taken after cooling down to room temperature. Following the evolution of the annihilation line parameters across the positron energy range [Fig. 4(a)] all three sample regions, i.e., oxidized surface, $Fe_{60}Al_{40}$ film, and the SiO_2 substrate, can be distinguished. The largest *S* variation is found in the nearest vicinity of the sample surface, where already at 400 °C the long disordered tail smoothens out due to annealing effects. For higher temperatures the *S* parameter in the surface region reaches its maximum at about 700 °C followed by a decrease with the subsequent temperature steps. For 1000 °C nearly the entire

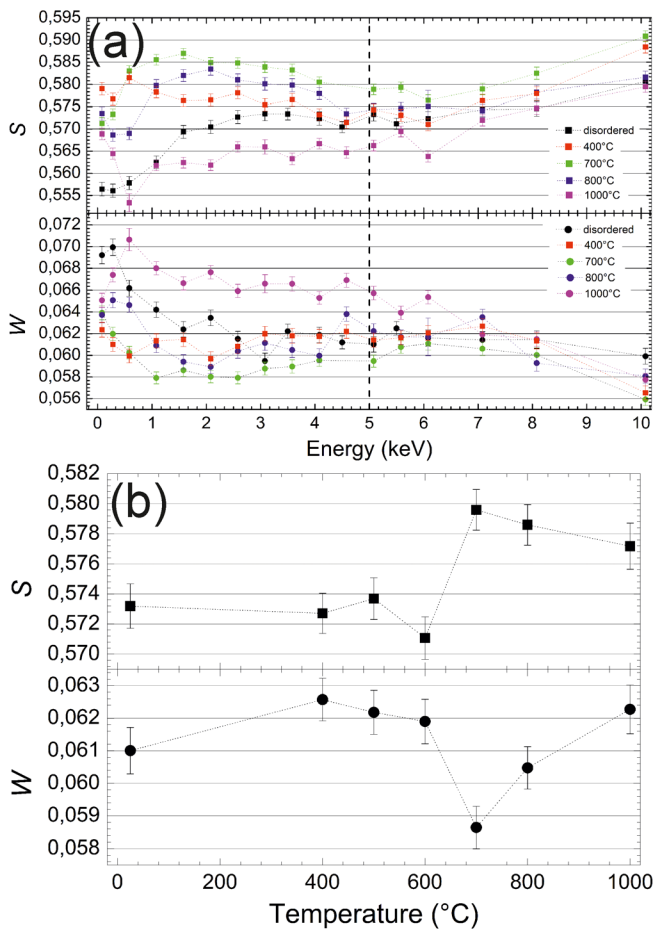

FIG. 4. Positron annihilation standard Doppler broadening annihilation line parameters *S* (squares) and *W* (dots) as a function of positron energy for different annealing temperatures measured at AIDA (a). Positron annihilation coincidence Doppler broadening parameters *S* (squares) and *W* (dots) as a function of temperature at 5 keV positron energy (marked with the vertical dotted line) measured at SPONSOR (b).

$S(E)$ curve is localized below the initial disordered sample curve that is likely due to the melting of the film, intermixing, secondary Fe phases creation as well as possible Al segregation as concluded from the XRD data. In general, for temperatures higher than 600 °C, the surface region extends to 3–4 keV, thus much wider as it has been found from the comparison between the ordered (furnace annealed) and disordered sample [see Fig. 3(b)]. That suggests possible increase of the oxidation layer thickness due to annealing. Since the increase of the oxide layer thickness takes place on the expense of the $Fe_{60}Al_{40}$ film, which consequently shrinks, larger data scattering in the S parameter for positron energies close to 5 keV are found. In order to overcome the low statistic problem cDB measurements at the positron energy of 5 keV were performed [see Fig. 4(b)]. The wing parameter W shows roughly an opposite trend to S along the overall positron energy range, however the data points scatter revealing the interpretation of defects decoration difficult.

cDB results are summarized in Figure 4(b), where the annihilation line parameters are plotted as a function of the annealing temperature. The data accumulation time for these kind of measurements is about two order of magnitude larger with respect to the overall number of counts in the region of interest (ROI) compare to the varied positron energy scans, about 10^7 counts compare to about 3×10^5 counts per energy step, respectively. We can clearly see that up to 600 °C both S and W parameters are more or less constant, whereas a jump followed by another plateau in the S parameter value for higher temperatures is visible. The jump of the S parameter can correspond to a slight increase of the open volume number and/or its size, whereas the decrease of W shifts the defect decoration in direction of Al. The S parameter difference at the jump is of about 1.5% that can be considered as low, nevertheless, a step-like dependence is visible. A drop of about 5.5% in W cannot be neglected. Moreover, W recovers to its original value at 1000 °C that suggests larger occupation of the neighboring defect sites with Fe as well as a slight change of film stoichiometry due to annealing.

In general, FeAl alloys contain relatively high concentration of vacancies which increases with increasing Al content, e.g., $Fe_{73}Al_{27}$ exhibits low concentration of vacancies[23] $c_V \approx 4 \times 10^{-6}$ while $Fe_{65}Al_{35}$ contains high vacancy concentration[24] of $c_V \approx 5 \times 10^{-3}$ that is of the same order, $c_V \approx 3 \times 10^{-3}$, as for $Fe_{64}Al_{36}$.[25] Thus, for our $Fe_{60}Al_{40}$ system we can expect the vacancy concentration of the 10^{-3} level. In addition, due to such a high concentration the positron diffusion length L_+ can be as low as 10 nm.[23] The vacancies are almost exclusively Fe-vacancies in the A sub-lattice. The concentration of vacancies in $Fe_{60}Al_{40}$ can become as high as 1 at. %, thus any variation in the concentration as a function of temperature at such elevated vacancies level are difficult to detect. The fact that magnetic phase transition do not reflect our cDB(T) results can imply: (i) basically no influence of the open volume on the transition itself or (ii) the amount of vacancies is too large thus the annihilation signal is saturated. The latter can be excluded since reasonably large changes of the annihilation line parameters as a function of temperature are found in the surface region of the $Fe_{60}Al_{40}$ film. In addition, it is unlikely that the surface region exhibits lower amount of open volume defects than the bulk thus is not saturated, whereas the bulk shows the saturation fingerprint.

D. CEMS

For the as-grown FeAl film, the Mössbauer spectra were deconvoluted into singlet and doublet lines associated with paramagnetic sites in the sample and a degenerated sextet related to a ferromagnetic fraction [Fig. 5(a)]. The relative areas of paramagnetic and ferromagnetic sites are estimated as ~42% and ~58%, respectively. The ferromagnetic phase of the sample could be explained by Fe atoms predominantly in a Fe surrounding. The mean hyperfine field is 15.1 T. This mean hyperfine field is by far lower than the hyperfine field of the α-Fe phase and could be interpreted as an existence of mixed environments inside the sample which are not implicated in the model. The paramagnetic phase could be described by the sum of a singlet and a doublet as in Bogner *et al.*,[14] where a single unsplit line is attributed to Fe surrounded by the largest number of Al atoms as in the ideal B2 structure, and the doublet can be associated with the Fe atoms having an Fe vacancy in the first coordination shell, which creates an electric field gradient (EFG).

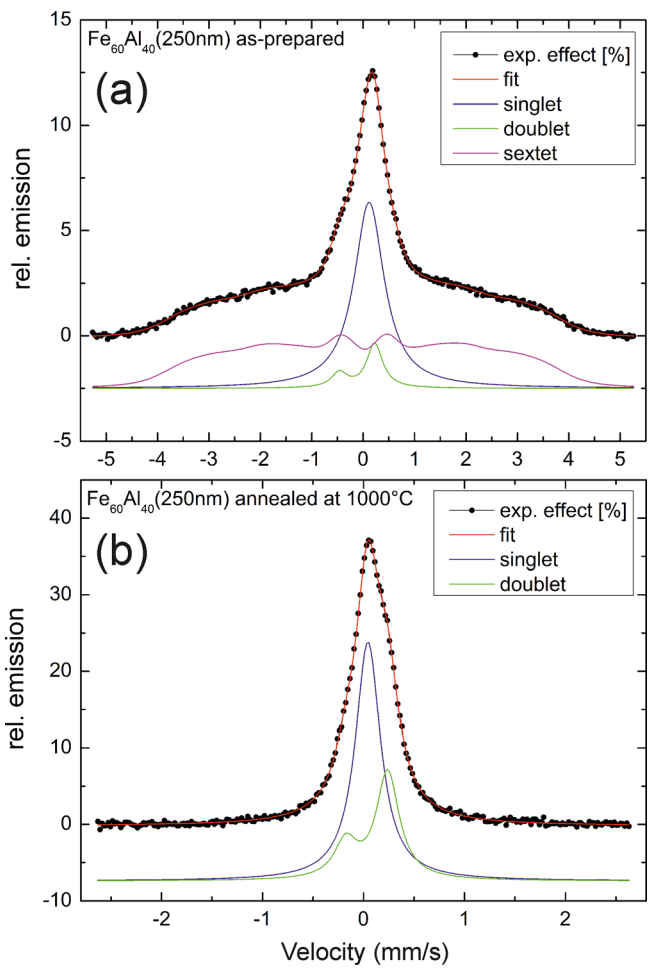

FIG. 5. Conversion Electron Mössbauer Spectroscopy results for the as-grown $Fe_{60}Al_{40}$ sample (a) and 1000 °C annealed (b) with corresponding fits.

Annealing of the FeAl films at 1000 °C temperatures leads to the disappearance of the sextet related to the hyperfine field and only a distorted single line is identified in the experimental data [Fig. 5(b)]. The spectrum could be decomposed into the singlet and doublet subspectra under the assumption that annealing leads to B2 ordering with vanishing magnetization. A visible difference in the line-shape of the central line compared to the as-grown film like a pronounced shoulder at the high-velocity side is found. The line widths of the subspectra and the quadrupole splitting are smaller in comparison to the as-grown film which suggests higher ordering in the annealed sample. This trend and the values of the fitting parameters are consistent with results of Bogner *et al.*[14] The ratio of the doublet/singlet areas changes from ~6/36 to ~35/65. A larger fraction of doublets in the subspectra of the annealed film could be explained by larger amount of thermal vacancies created at high temperature or further quenching.[26] Probably, regions with EFG are redistributed within the film leading to more pronounced texture as in the as-prepared sample.

IV. CONCLUSIONS

In conclusion, we have shown that thermal annealing of the $Fe_{60}Al_{40}$ chemically disordered films governs expected magnetic phase transition from the ferromagnetic A2-phase into paramagnetic ordered B2-phase that shows no visible dependence on the open volume defects as a result of the cDB investigations. The magnetic phase transition is usually fully accomplished at 500–600 °C, where no visible changes of the annihilation line parameters have been observed. Still, in the surface region of the sample reasonably large annihilation line parameters variations have been found showing sufficient sensitivity of our experimental tools, and ruling out possible signal saturation due to too high vacancies concentration. At higher temperatures, a slightly larger defect concentration as well as different defect decorations were found that is likely a result of temperature driven material decomposition leading to a complete film melt at 1000 °C. Magnetic and structural changes have been tracked using PAS, XRD, and CEMS measurements. The magnetic phase transition from para- to ferro-magnetic behavior appears to be driven by chemical disordering alone, and is independent of the vacancy concentration. On the other hand decrease of the lattice parameter upon annealing suggests importance of stress for the magnetic phase transition. These results help understand the role of defects in materials that show disorder-induced ferromagnetism.

ACKNOWLEDGMENTS

This work has been partially financed by the Initiative and Networking Fund of the German Helmholtz Association, Helmholtz Virtual Institute MEMRIOX (VH-VI-442), and by Stiftung Mercator (MERCUR).

[1]J. H. Westbrook and R. L. Fleischer, *Properties and Applications of Intermetallic Compounds: Structural Applications, Intermetallic Compounds* (John Wiley & Sons, New York, 2000), Vol. 3.
[2]J. Nogués, E. Apiñaniz, J. Sort, M. Amboage, M. d'Astuto, O. Mathon, R. Puzniak, I. Fita, S. Garitaonandia, S. Suriñach, J. S. Muñoz, M. D. Baró, F. Plazaola, and F. Baudelet, Phys. Rev. B **74**, 024407 (2006).
[3]H. Gengnagel, M. J. Besnus, and H. Danan, Phys. Status Solidi A **13**, 499 (1972).
[4]X. Amils, J. Nogués, S. Suriñach, J. S. Muñoz, M. D. Baró, A. Hernando, and J. P. Morniroli, Phys. Rev. B **63**, 052402 (2001).
[5]A. Taylor and R. M. Jones, J. Phys. Chem. Solids **6**, 16 (1958).
[6]J. Fassbender, M. O. Liedke, T. Strache, W. Möller, E. Menéndez, J. Sort, K. V. Rao, S. C. Deevi, and J. Nogués, Phys. Rev. B **77**, 174430 (2008).
[7]E. Menéndez, M. O. Liedke, J. Fassbender, T. Gemming, A. Weber, L. J. Heyderman, K. V. Rao, S. C. Deevi, S. Suriñach, M. D. Baró, Jordi Sort, and J. Nogués, Small **5**, 229 (2009).
[8]A. Hernando, X. Amils, J. Nogués, S. Suriñach, M. D. Baró, and M. R. Ibarra, Phys. Rev. B **58**, R11864 (1998).
[9]E. Menéndez, J. Sort, M. O. Liedke, J. Fassbender, S. Suriñach, M. D. Baró, and J. Nogués, New J. Phys. **10**, 103030 (2008).
[10]J. Sort, A. Concustell, E. Menéndez, S. Suriñach, K. V. Rao, S. C. Deevi, M. D. Baró, and J. Nogués, Adv. Mater. **18**, 1717 (2006).
[11]G. K. Wertheim, V. Jaccarino, J. H. Wernick, and D. N. E. Buchanan, Phys. Rev. Lett. **12**, 24 (1964).
[12]R. Bali, S. Wintz, F. Meutzner, R. Hübner, R. Boucher, A. A. Ünal, S. Valencia, A. Neudert, K. Potzger, J. Bauch, F. Kronast, S. Facsko, J. Lindner, and J. Fassbender, Nano Lett **14**, 435 (2014).
[13]X. Amils, J. Nogués, S. Suriñach, M. D. Baró, and J. S. Muñoz, IEEE Trans. Magn. **34**, 1129 (1998).
[14]J. Bogner, W. Steiner, M. Reissner, P. Mohn, P. Blaha, K. Schwarz, R. Krachler, H. Ipser, and B. Sepiol, Phys. Rev. B **58**, 14922 (1998).
[15]J. Wolff, M. Franz, A. Broska, B. Köhler, and T. Hehenkamp, Mater. Sci. Eng. A **239–240**, 213 (1997).
[16]J. Kansy, A. Hanc-Kuczkowska, and D. Giebel, Nukleonika **58**, 221 (2013), available at http://www.nukleonika.pl/www/back/full/vol58_2013/v58n1p221f.pdf.
[17]W. Anwand, H.-R. Kissener, and G. Brauer, Acta Phys. Polonica A **88**, 7 (1995), available at http://przyrbwn.icm.edu.pl/APP/PDF/88/a088z1p01.pdf.
[18]W. Anwand, G. Brauer, M. Butterling, H. R. Kissener, and A. Wagner, Defect Diffus. Forum **331**, 25 (2012).
[19]M. Potesser, T. Schoeberl, H. Antrekowitsch, and J. Bruckner, in *EPD Congress 2006: TMS (The Minerals, Metals & Materials Society), San Antonio, USA, 12–16 March 2006*, edited by S. M. Howard, R. L. Stephens, C. J. Newman, J.-Y. J. Hwang, A. M. Gokhale, T. T. Chen, T. P. Battle, M. L. Free, B. R. Davis, C. L. Harris, H. Henein, P. N. Anyalebechi, A. C. Powell, G. K. Krumdick, and C. K. Bel (Curran Associates, Inc., New York, 2006), pp. 167–176.
[20]R. Krause-Rehberg and H. Leipner, *Positron Annihilation in Semiconductors, Solid-State Sciences* (Springer, Berlin, 1999), Vol. 127.
[21]A. F. Makhov, Sov. Phys. Solid State **2**, 2172 (1961).
[22]O. Melikhova, J. Čížek, I. Procházka, J. Kuriplach, F. Lukáč, M. Cieslar, G. Brauer, and W. Anwand, Phys. Status Solidi C **6**, 2367 (2009).
[23]F. Lukáč, J. Čížek, I. Procházka, Y. Jirásková, D. Janičkovič, J. Šimeg Veterníková, W. Anwand, and M. Butterling, J. Phys.: Conf. Series **505**, 012013 (2014).
[24]F. Lukáč, J. Čížek, I. Procházka, Y. Jirásková, D. Janičkovič, W. Anwand, and G. Brauer, J. Phys.: Conf. Series **443**, 012025 (2013).
[25]J. Wolff, M. Franz, A. Broska, R. Kerl, M. Weinhagen, B. Köhler, M. Brauer, F. Faupel, and T. Hehenkamp, Intermetallics **7**, 289 (1999).
[26]M. Zhao, K. Yoshimi, K. Maruyama, and K. Yubuta, Acta Mater. **64**, 382 (2014).